Theoretical and Experimental Investigation of Using Multidegree of Freedom Electrostatically Actuated Microstructures in Performing Classification Problems

Hamed Nikfarjam, *Member, IEEE*, Mohammad Megdadi, Mohammad Okour, Siavash Pourkamali, *Senior Member, IEEE*, and Fadi Alsaleem

***Abstract*—This article demonstrates the use of micro-electromechanical systems (MEMS) to perform an efficient classification problem. Classification using digital computers is inefficient due to its power requirement and the separation between memory and processing units. As a proof of concept, the basic signal classification has been performed using a network of only three mechanically coupled devices. The classification has occurred at the hardware level rather than using a digital computer. The classification problem involves distinguishing between a ramp signal and a step input signal. In this demonstration, a three-degree-of-freedom model was built for the proposed network in MATLAB. The detailed simulation results were extracted to validate the network operation and sensitivity to operating conditions. Next, the device network hardware was fabricated and tested to perform the required classification problem. Good agreement between simulation and experiment is demonstrated.**

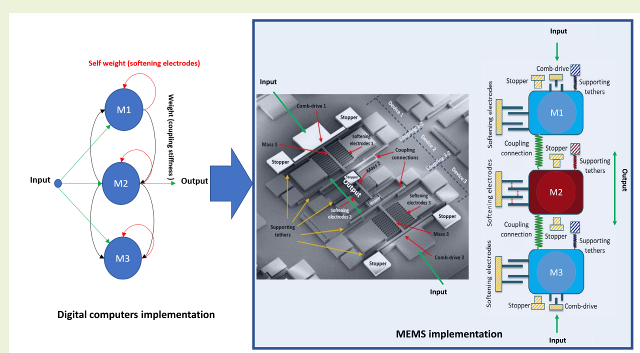

***Index Terms*—Mechanical computing, mechanical coupling, micro-electromechanical systems (MEMS), neuromorphic computing, parallel-plate actuators, pull-in, signal classification.**

I. Introduction

DUE to the increasing demand for computational speed and complexity for applications such as neural computing and artificial intelligence, and the inevitable end of Moore's law eventually [1], a technology that compensates for the no-longer-existing miniaturizing of transistors is highly needed. The high power consumption and complicated thermal management requirements of existing CMOS-based technologies have become additional bottlenecks. Recently, considerable attention has been given to electrostatically actuated micro- and nano-electromechanical systems (MEMS/NEMS) to expand their typical use as high-frequency switches [2], sensors [3], radio frequency (RF) switches [4], mirrors [5], and oscillators [6] to be the next memory [7] and logic gate devices [8]. Their low power consumption [8], [9], near-zero leakage power [8], and ability to survive a harsh operating environment over CMOS are the main driving motivations behind this interest [9]. However, while contact surface wearing [10] and stiction [11], [12] issues have limited the use of MEMS/NEMS switches as potential logic gates, the introduction of non-contact MEMS resonators has received some attention [8]. In this scenario, the resonator's high oscillation amplitude is considered the logic value 1, and its low oscillation amplitude is the logic value 0. Operating linearly, near nonlinear regimes, such as parametric and secondary resonances [13] and thermal modulation [8], are among the methods suggested to achieve the Boolean electrostatic MEMS/NEMS resonator-based gate. However, state-of-the-art electrostatically driven MEMS resonators have significant limitations in the range of deflection due to the separation between electrodes, instability regions, and high operating voltages [13], [14]. Moreover, most of the above-proposed methods to realize logic MEMS-based gates require strictly fixed frequencies and different output and input frequencies. They suffer significant voltage attenuation while

Manuscript received 7 March 2023; accepted 5 April 2023. Date of publication 13 April 2023; date of current version 31 May 2023. This work was supported by the National Science Foundation under Grant 1935598 and Grant 935641. The associate editor coordinating the review of this article and approving it for publication was Dr. Yong Zhu. *(Corresponding author: Fadi Alsaleem.)*

Hamed Nikfarjam and Siavash Pourkamali are with the Department of Electrical Engineering and Computer Sciences, The University of Texas at Dallas, Richardson, TX 75080 USA.

Mohammad Megdadi is with the Department of Mechanical Engineering, University of Nebraska–Lincoln, Lincoln, NE 68588 USA.

Mohammad Okour and Fadi Alsaleem are with the Department of Architectural Engineering, University of Nebraska–Lincoln, Lincoln, NE 68588 USA (e-mail: falsaleem2@unl.edu).

Digital Object Identifier 10.1109/JSEN.2023.3265908

1558-1748 © 2023 IEEE. Personal use is permitted, but republication/redistribution requires IEEE permission.
See https://www.ieee.org/publications/rights/index.html for more information.

Authorized licensed use limited to: University of Nebraska Omaha Campus. Downloaded on November 06,2023 at 19:05:53 UTC from IEEE Xplore. Restrictions apply.

transferring energy from one logic gate to another [15]. Hence, stability issues, high voltage activation, and poor cascading compatibility are considered significant challenges limiting the adoption of electrostatic MEMS into logic gate design. In addition, due to the small size that transistors have reached, building a complete digital logic gate from a single MEMS structure requires the same or more space than the number of transistors needed to perform the same logic.

On the other hand, alternative computing paradigms are not based on logic gates, such as biologically inspired neuromorphic computing [16]. Neuromorphic computers utilize physical hardware to perform computing rather than a digital circuit. In this regard, electrostatic MEMS devices have shown potential in performing at least two types of neuromorphic computing approaches: the traditional neural network (NN)-based [15], [17], [18], [19], [20] and reservoir computing (RC) [21], [22], [23], [24] approaches. Compared to the NN, MEMS development in RC is more mature in the literature. Several studies have reported experimental validation for MEMS-based RC solutions in many applications, such as signal [21] and spoken language [22] classifications. However, RC generally requires a postprocessing step that may need some digital computing power. Moreover, the MEMS RC approach reported in the literature is based on the RC virtual node concept that requires serial processing, which is often slower than the parallel computing approach in NN.

In the NN neuromorphic MEMS approach, the equation governing electrostatic MEMS devices has been shown recently to be very similar to the neuron equation of a recurrent NN (RNN) [19]. Thus, an MEMS can naturally capture neuron behavior in a single device. When coupled with other MEMS devices, this forms a physical RNN network with the promise of producing integrated neural circuits with brain-like functionality [15], [21]. Such a network does not require any postprocessing and performs computing in a fast parallel fashion without needing a digital computer. The dynamic complexity of coupled electrostatic MEMS devices, a key to this computing approach, has received significant attention in the literature. For example, an analytical framework for analyzing large-scale arrays of coupled MEMS devices was presented in [25].

Moreover, the connected MEMS-based Colpitts devices were exploited in [26], and finally, the modal characteristics of the dynamics of MEMS-coupled resonators were investigated in [27]. However, most of the focus in the literature was on utilizing such complexity to enhance the MEMS used as a sensor, such as its bandwidth [28], selectivity [29], and sensitivity [30]. One of the few works on using the complexity of a network of coupled MEMS devices for computing purposes is dated back to 2001 [17]. In this work, the authors explored the potential of using a network of coupled MEMS devices as an NN neuromorphic computer for the first time. It was shown, using simulation, that a network of electrostatic MEMS devices with specific oscillatory patterns and phase relationships could produce some computing capabilities. This work built on the author's previous demonstration that generally coupled resonators with complex dynamics is shown to have associative memory when coupled appropriately [31]. However, it took more than 16 years for another group to confirm such MEMS computing capabilities and demonstrate them theoretically in a pattern recognition application [18].

Despite the computing potential of coupled MEMS devices in realizing NN computers, most of the MEMS computing works in the literature are based on simulation models. It needs hardware demonstration of such computing capabilities [17], [18]. Moreover, very generic models for the MEMS devices were used in this simulation. Such models deal with electrostatic MEMS as a generic differential equation that does not account for MEMS physical operation and design parameters such as the excitation method and coupling characteristics. This article overcomes these challenges by presenting: 1) the first detailed model of a network of electrostatically actuated microstructures designed for NN computing purposes and 2) a hardware implementation guided by this model to perform a real-time signal classification problem. This hardware has great potential to overcome the current limitations of digital computing in solving classification problems. Specifically, this hardware comprises electrostatic MEMS devices that consume power in the nanowatt range [15]. To solve a similar classification problem using a digital computer that implements Python code algorithms, at least 10 000 transistors must be switched during a single floating operation [16] and consume power in the milliwatt range [15].

II. Working Principle

Classification is one of the most popular tasks in machine learning literature. Using simulation, we have previously shown a simple classification task as a test for the computational potential of a network of MEMS devices [20]. The task involves the nontrivial problem in [32] to classify an input waveform into either a "Step" signal or a "Ramp" signal. In this classification task, input waveforms are supposed to be applied as a voltage signal to the MEMS network. For the MEMS network to perform the computational task correctly, the size of the network and the bias voltages and connection weights values between the MEMS devices need to be optimized.

In this article, we demonstrate this classification problem using a customized MEMS hardware design that eliminates the need for any circuit to perform the task [33]. A schematic of this hardware is shown in Fig. 1 and requires a minimum of three MEMS devices forming a network that resembles an NN of three neurons. The upper and lower masses are the input devices that receive the input signal (I_1 and I_2 in the figure), while the third MEMS device forms the output (O) layer, which is also the middle mass, and its status decides the class of the input signal. The MEMS neurons are coupled together mechanically by springs. The spring stiffness values resemble the weights of a typical NN. Each MEMS device has additional parallel-plate electrodes to bias the device from its rest by applying constant bias voltages. The bias voltage is used to shift the MEMS mass toward the pull-in. If no bias voltages were applied, the proof mass response would be almost linear

Authorized licensed use limited to: University of Nebraska Omaha Campus. Downloaded on November 06,2023 at 19:05:53 UTC from IEEE Xplore. Restrictions apply.

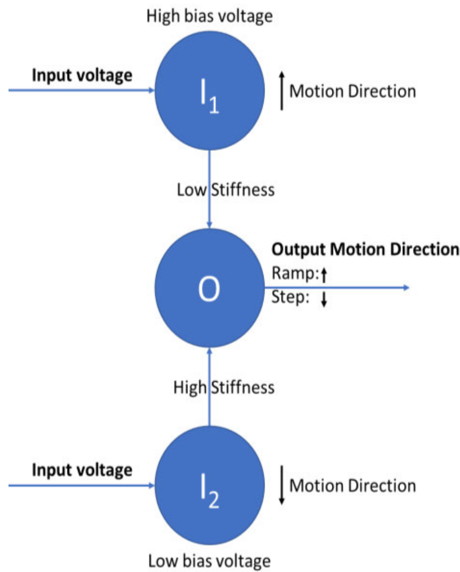

Fig. 1. Sample MEMS architecture to perform the simple signal classification problem.

when the input signal is applied. Thus, having no bias voltage reduces the MEMS network computing capabilities. Finally, each MEMS in the network is designed to have a different bias voltage value. Thus, besides weights, the bias voltage is another tuning parameter that can be adjusted to perform our classification task or other classification tasks.

The expected operation for the hardware to distinguish between two different signal shapes is: if a ramp input voltage is applied, the output mass pulls in upward, while if a step signal is applied, the output mass pulls in downward. There are two requirements to achieve this behavior.

(R1): The coupling spring stiffness between the lower and middle masses has to be greater than the upper to middle mass coupling spring stiffness (i.e., the lower input mass has a more significant impact on the middle output mass).

(R2): The bias voltage plus the input signal for the upper mass is higher than the lower mass, so it pulls in at a lower input voltage. In this manner, if a step input is applied, the upper and lower masses will pull in almost simultaneously, but the middle mass will follow the lower (stronger coupling) mass and pull in downward.

On the other hand, if a ramp signal is applied, as the voltage gradually increases, the upper mass will pull in first due to its higher bias voltage, and the middle mass will follow by pulling upward. Once in this state, even if the ramp input keeps increasing and the lower mass eventually pulls in, due to hysteresis in the parallel-plate actuator behavior (memory), the resulting downward force is not enough to pull the middle mass out of its upward pulled-in position. The complete classification operation is shown in Fig. 2 with actual design parameters to perform the required classification.

III. Modeling and Fabrication

The computing hardware comprises three MEMS neurons coupled together mechanically to accomplish the classification task. The system layout consists of an input layer with two MEMS with big proof masses and an output layer with one mass in the middle. The system can be modeled as a three-free-degree-of-freedom model, as shown in Fig. 3(a). In this model, each proof mass is surrounded by several fingers acting as parallel-plate electrostatic actuators. When a bias voltage is applied, the parallel-plate actuators labeled as "softening electrodes" induce a negative electrostatic stiffness, lowering the structure's stiffness while making the force–displacement characteristics of the moving elements highly nonlinear imitating the nonlinear behavior of biological neurons [19]. The input signal is applied through comb-drive electrostatic actuators that can exert displacement-independent input forces to the moving elements upon application of an input voltage. Once an input voltage is applied, the input masses will be attracted and move toward their comb-drive actuator; the upper mass moves up and the lower mass moves down. As the voltage increases, the attraction force and displacement increase, reducing the gap between the softening electrodes. At some threshold voltage, the softening electrodes attached to the mass reach the point of instability where the mass moves abruptly toward the stopper and collides with it (pull-in). This pull-in behavior is a well-known characteristic of parallel-plate electrostatic actuators. The stoppers positioned between the mass and the comb drive prevent direct contact between the charged electrodes upon pull-in. The displacement of the input proof masses leads to displacement of the output proof mass (the mass in the middle) due to the existing mechanical coupling (springs) between the proof masses. The output proof mass can pull-in in either direction, determining the classification task's result.

The following equations of motions that govern the system dynamics in Fig. 3 were simulated in MATLAB:

$$M\ddot{X} + C\dot{X} + KX = \boldsymbol{F_{CD}} + \boldsymbol{F_{PP}} \tag{1}$$

where $\boldsymbol{X}$ is the relative displacement matrix of the three masses and M, C, and K are the matrix form of the system's masses, damping constants, and stiffnesses, respectively, defined as

$$\boldsymbol{X} = \begin{bmatrix} x_1 \\ x_2 \\ x_3 \end{bmatrix}, \quad M = \begin{bmatrix} m_1 & 0 & 0 \\ 0 & m_2 & 0 \\ 0 & 0 & m_3 \end{bmatrix}$$
$$C = \begin{bmatrix} c_1 & 0 & 0 \\ 0 & c_2 & 0 \\ 0 & 0 & c_3 \end{bmatrix}$$
$$K = \begin{bmatrix} k_1 + k_{12} & -k_{12} & 0 \\ -k_{12} & k_2 + k_{12} + k_{32} & -k_{32} \\ 0 & -k_{32} & k_3 + k_{32} \end{bmatrix}. \tag{2}$$

$\boldsymbol{F_{CD}}$ is the attractive electrostatic force from the comb-drives and $\boldsymbol{F_{PP}}$ is the electrostatic force from the parallel plates. The electrostatic force of a typical parallel-plate MEMS is given by: $F_e = (\varepsilon A V^2/g)$, where A is the overlapping area between the electrodes, V is the voltage difference between them, and g is the gap distance between them. Using this equation, one can develop the expressions for $\boldsymbol{F_{CD}}$ and

Authorized licensed use limited to: University of Nebraska Omaha Campus. Downloaded on November 06,2023 at 19:05:53 UTC from IEEE Xplore. Restrictions apply.

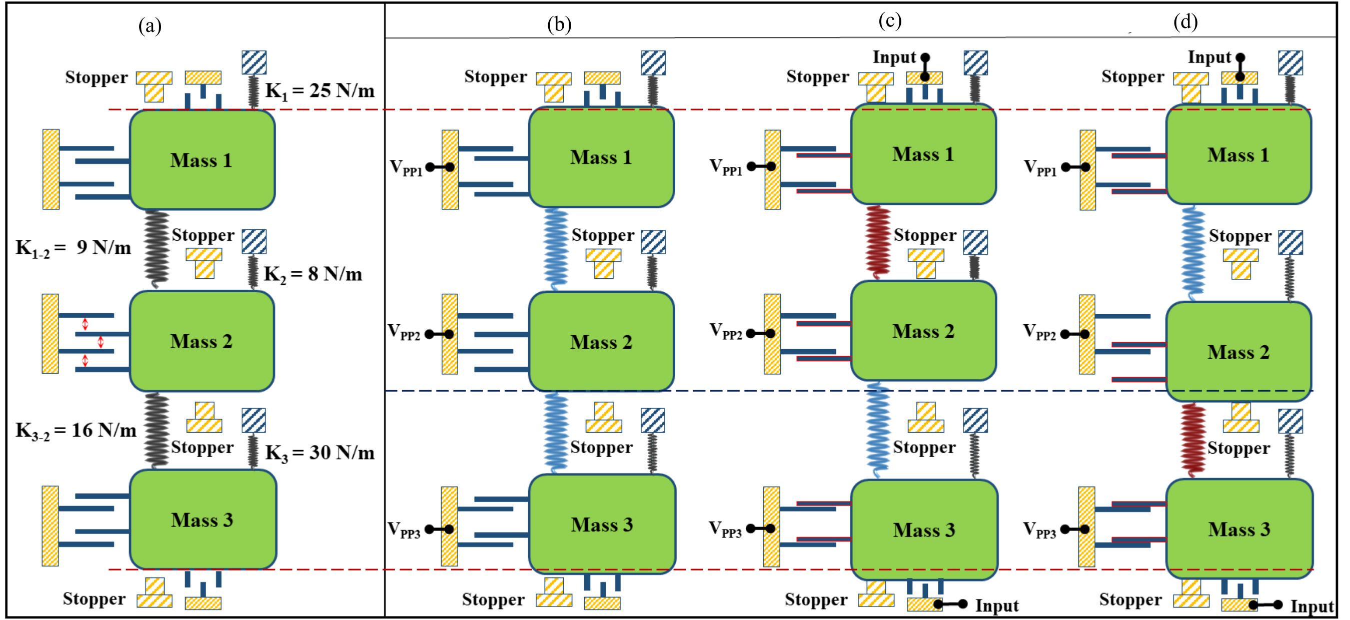

Fig. 2. Schematic views of the three coupled MEMS devices operating to perform the required signal classification task. (a) Devices are at rest. (b) Bias voltages are applied to the softening electrodes bringing the three elements close to the pull-in/instability point. (c) Gradually increasing (ramp) input voltage applied to comb drives; M2 pulled toward M1 upon M1 pull-in; eventually, M3 will pull in, but due to strong hysteresis in the parallel-plate electrostatic force (memory), M2 will not release. (d) Abrupt voltage applied to comb drives, M1 and M3 pulling in simultaneously and M2 moving toward M3 due to stiffer coupling element.

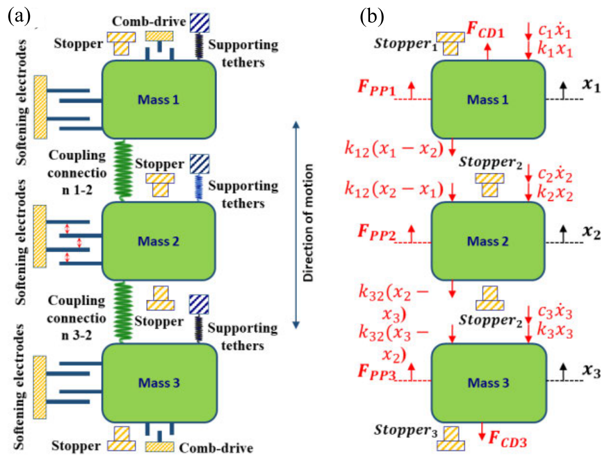

Fig. 3. (a) Three degrees of freedom coupled MEMS system. (b) System's free body diagram.

$\boldsymbol{F_{PP}}$ as follows [35]:

$$\boldsymbol{F_{CD}} = \begin{bmatrix} F_{\text{CD1}} \\ 0 \\ -F_{\text{CD3}} \end{bmatrix}, \quad \boldsymbol{F_{PP}} = \begin{bmatrix} F_{\text{PP1}} \\ F_{\text{PP2}} \\ F_{\text{PP3}} \end{bmatrix} \tag{3}$$

where

$$F_{\text{CD1}} = N_{\text{CD1}}\varepsilon t V_{\text{CD1}}^2 \left(\frac{1}{g_{\text{CD1}}} + \frac{w_{\text{CD1}}}{(d_{\text{CD1}} - x_1(t))^2} \right) \tag{4}$$

$$F_{\text{CD3}} = N_{\text{CD3}}\varepsilon t V_{\text{CD3}}^2 \left(\frac{1}{g_{\text{CD3}}} + \frac{w_{\text{CD3}}}{(d_{\text{CD3}} + x_3(t))^2} \right) \tag{5}$$

$$F_{\text{PP}i} = \frac{1}{2} N_{\text{PP}i}\varepsilon t L_{\text{PP}i} V_{\text{PP}i}^2 \times \left(\frac{1}{(d_{\text{PPU}i} - x_i(t))^2} - \frac{1}{(d_{\text{PPL}i} + x_i(t))^2} \right), \quad i = 1, 2, 3 \tag{6}$$

where the parameters in (1)–(6) and their values are presented in Table I (Appendix).

A basic single-mask SOI micromachining process was used to fabricate the devices on a p-type SOI substrate with a 50-μm-thick silicon device layer and a 2-μm-thick buffer oxide layer (BOX). The device layer was first patterned via an optical lithography step, and the structures were carved out of the SOI device layer via deep reactive ion etching (DRIE) to the BOX. The BOX layer was then removed underneath narrower features by a timed hydrofluoric acid etch to suspend the structures. The structure was then dried using the naphthalene drying method explained in [34].

IV. Results

A model for the system in Fig. 2 and presented in (2)–(6) was simulated in MATLAB to validate the classification operation. The input signal that fed the lower mass was scaled by a factor of $R_{\text{CD}} = V_{\text{CD3}}/V_{\text{CD1}} = 0.82$ to satisfy R2. The parallel plates of the three masses were biased with voltages near their instability region. As shown in Fig. 4(a), if a ramp input voltage is applied, the upper mass pulls in first, and the middle mass follows and pulls upward. Even when the ramp signal reaches a point where the lower input mass pulls in, the middle mass remains pulled upward. On the other hand, as expected, the middle mass pulls in downward if a step input voltage with a high voltage is applied [see Fig. 4(b)].

Next, the classification sensitivity against operation parameters, such as the bias voltage for each MEMS ($V_{\text{PP}i}$), the input

Authorized licensed use limited to: University of Nebraska Omaha Campus. Downloaded on November 06,2023 at 19:05:53 UTC from IEEE Xplore. Restrictions apply.

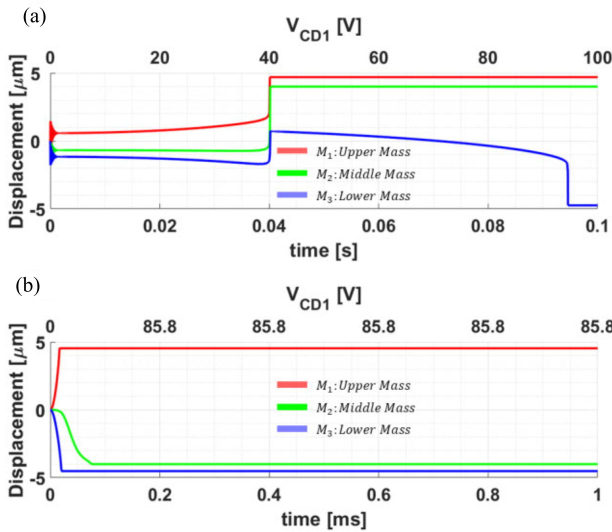

Fig. 4. MEMS computing unit performance under different input signals. The deflection of the three MEMS when (a) ramp input and (b) step input signal are applied.

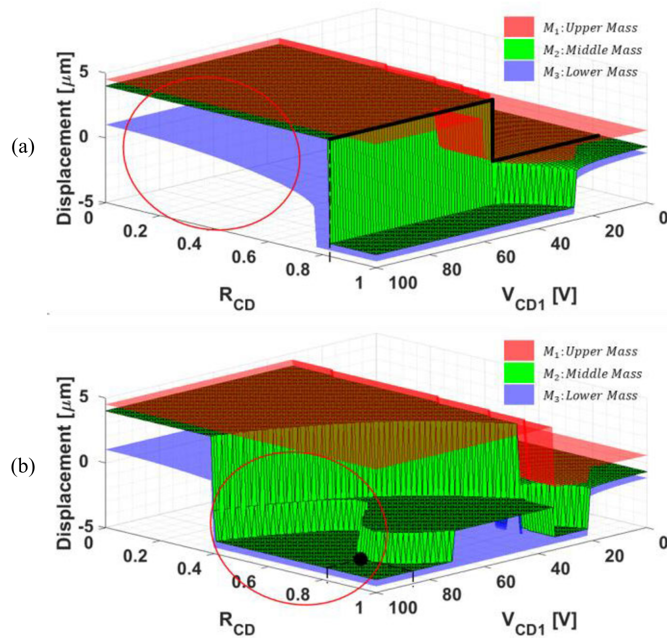

Fig. 5. Three-dimensional plots for the MEMS network response when (a) ramp and (b) step input signals are applied while varying the input voltage V_{CD1} and the ratio R_{CD}. The circle indicates the working range for each input signal.

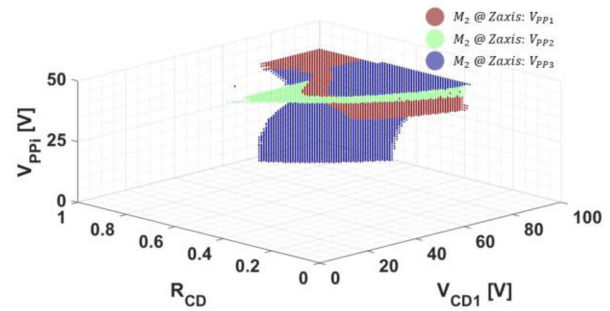

Fig. 6. High-dimensional plot showing the operation voltages that result in a working classification. Each point in the plot represents the case when the middle mass pulls in upward if a ramp input is applied and downward if a step input is applied. The *y*-axis is the bias voltage value for a given MEMS.

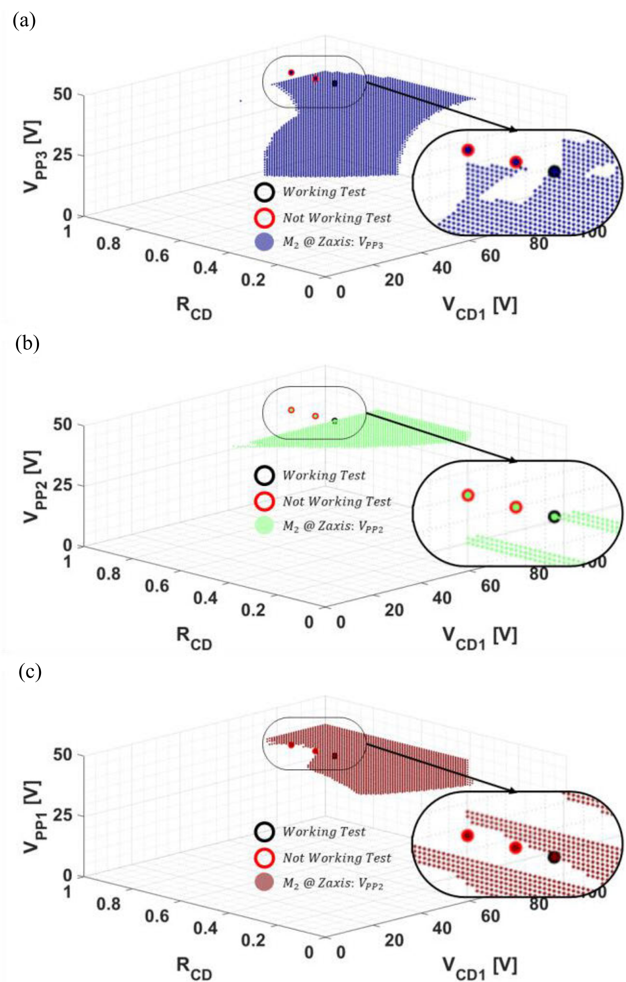

Fig. 7. Extracted plots from Fig. 6 showing the working voltage ranges to produce the correct classification when varying only: (a) MEMS 3 voltage, (b) MEMS 2 bias voltage, and (c) MEMS 1 bias voltage. The black circled dots present working experimental data, while the red is not working data.

voltage on the comb drives of each ($V_{\text{CD}i}$), where $i = 1$, 2, and 3 is an index representing each MEMS in the network, and the voltage ratio R_{CD} of the comb-drive voltage between the upper and lower MEMS devices ($R_{\text{CD}} = V_{V_{\text{CD3}}/V_{\text{CD1}}}$), was investigated. The 3-D plots in Fig. 5 show the effect of varying the amplitude of the two comb-drive voltages. Fig. 5(a) shows the pull-in upward range of the middle mass for a ramp input and Fig. 5(b) for a step input. Fig. 5(b) shows that the input voltage must start with no less than 35 V ($V_{\text{CD1}} > 60$ V) to perform the classification. Moreover, the working range of R_{CD} to classify a step input signal (i.e., middle mass pulling down) ranging from $R_{\text{CD}} = 0.40$ to 1. However, only $R_{\text{CD}} < 0.82$ is the operating range to classify the ramp input signal (i.e., middle mass pulling up). Thus, $0.40 < R_{\text{CD}} < 0.82$ is the operating range to satisfy both classification conditions.

Authorized licensed use limited to: University of Nebraska Omaha Campus. Downloaded on November 06,2023 at 19:05:53 UTC from IEEE Xplore. Restrictions apply.

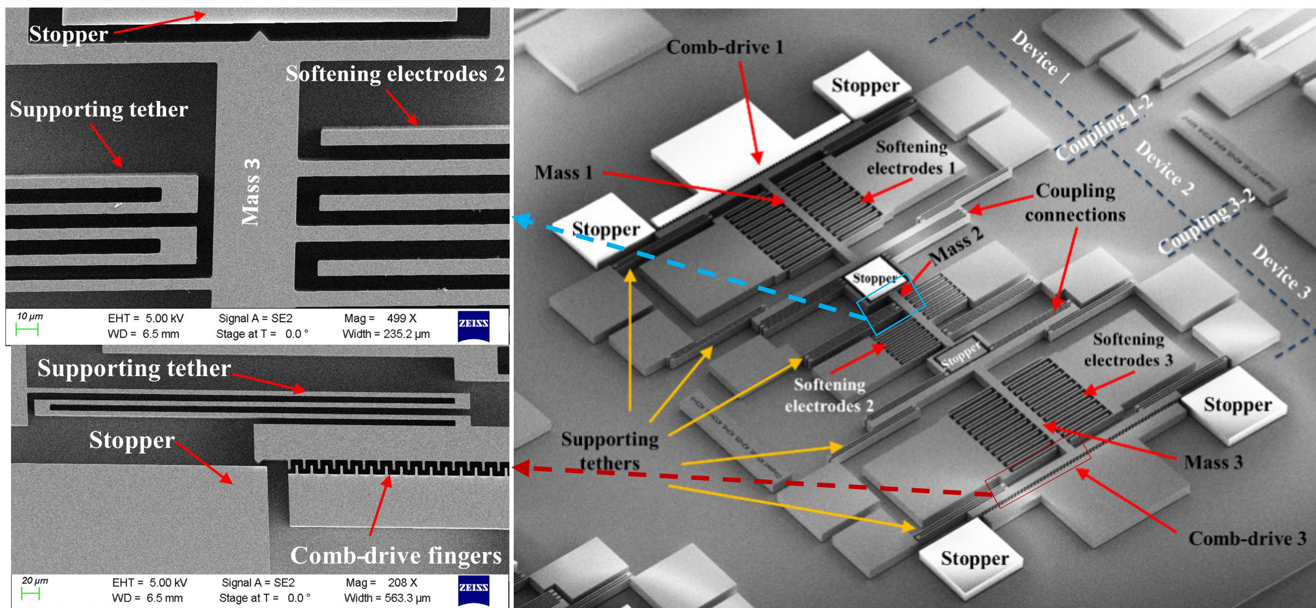

Fig. 8. SEM view of the fabricated device and details of the device structure.

A further sensitivity investigation of the MEMS network was done by varying the bias voltages V_{PP} of each mass. A higher dimension plot is presented in Fig. 6. To interpret this plot better, its derivatives, varying only one MEMS mass bias at a time, are shown in Fig. 7(a)–(c). In these figures, to achieve the displayed higher plot dimensionality than the traditional 3-D plot, we followed the following novel approach: 1) only present the desired status of the (output) middle mass; 2) use distinctive colors to represent the effect of varying the bias voltage of each mass; and 3) when varying the bias voltage of a mass, bias voltage of other masses was kept the other masses bias voltage at a constant value close to the mass pull-in voltage. Adopting this approach, each dot point in these figures represents the corresponding input voltage, input voltage ratio, and bias voltage for a given mass so that the middle mass pulls in upward if a ramp input is applied and downward if a step input is applied. Moreover, a red dot represents the effect of only varying the bias voltage of the upper mass (V_{PP1}), a green dot represents the effect of only varying the bias voltage of the middle mass (V_{PP2}), and a blue dot represents the effect of only varying the bias voltage of the lower mass (V_{PP3}).

The higher dimension plots provide easy visualization to conclude the required operating voltages to achieve the desirable classification task. For example, one can notice that the operation of the network is susceptible to the bias voltage of the middle mass. Moreover, the lower mass has a wide operation range for its bias voltage compared to the rest of the masses to achieve the required classification. Finally, the higher dimensional plots confirm that higher input voltage values and ratios are desirable for performing the required classification.

A neural computing unit comprised of three micromachined components, similar to the one shown in Fig. 2, was fabricated to validate the simulation results. A scanning electron microscope (SEM) view of a fabricated network is shown in Fig. 8. Each coupled element consists of one suspended, "I" shaped proof mass supported by two or four meandering tethers. Each mass has two arrays of electrodes extending outward, forming parallel-plate electrostatic actuators with adjacent arrays of fixed electrodes to form the softening actuators. The coupling connection between masses 3 and 2 is stiffer than masses 3 and 1 to create a downward pull-in in element 2 in case of a step input but not stiff enough to pull element 2 out of an upward pull-in in case of a ramp input.

A sample operation voltage condition, represented by black circled dots in Fig. 7, was chosen to validate the simulation model. The corresponding bias voltages values are V_{PP1} = 33 V, V_{PP2} = 34 V, and V_{PP3} = 38 V and the ratio between the two comb drives was set to R_{CD} = 0.82. R_{CD}, which is very close to the edge of the operation range to validate the system sensitivity. Fig. 9(b) shows the system's resting position after applying the bias voltages to the softening parallel-plate actuators. When a ramp input is applied, at V_{CD1} = 34.1 V, the upper mass pulls in and pulls the middle mass upward along with it [see Fig. 9(c)]. When the voltage is further increased and reached V_{CD1} = 71 V, the lower mass also pulls in, trying to pull the middle mass downward [see Fig. 9(d)]. However, this action is insufficient to release the middle mass from its current upward pulled-in state (due to the hysteresis). On the other hand, as expected from the simulation, from the rest position, the middle mass pulls in downward if a step input voltage of V_{CD1} = 72 V is suddenly applied to the comb drives [see Fig. 9(e)]. The successful operation of the network was also verified with other voltages within the suggested operation range of the simulation. More importantly, it was verified that choosing values outside (red circled dots in Fig. 7) of the operation range suggested by simulation resulted in false classification. For example, with the same voltages implemented in Fig. 9 and by just increasing

Authorized licensed use limited to: University of Nebraska Omaha Campus. Downloaded on November 06,2023 at 19:05:53 UTC from IEEE Xplore. Restrictions apply.

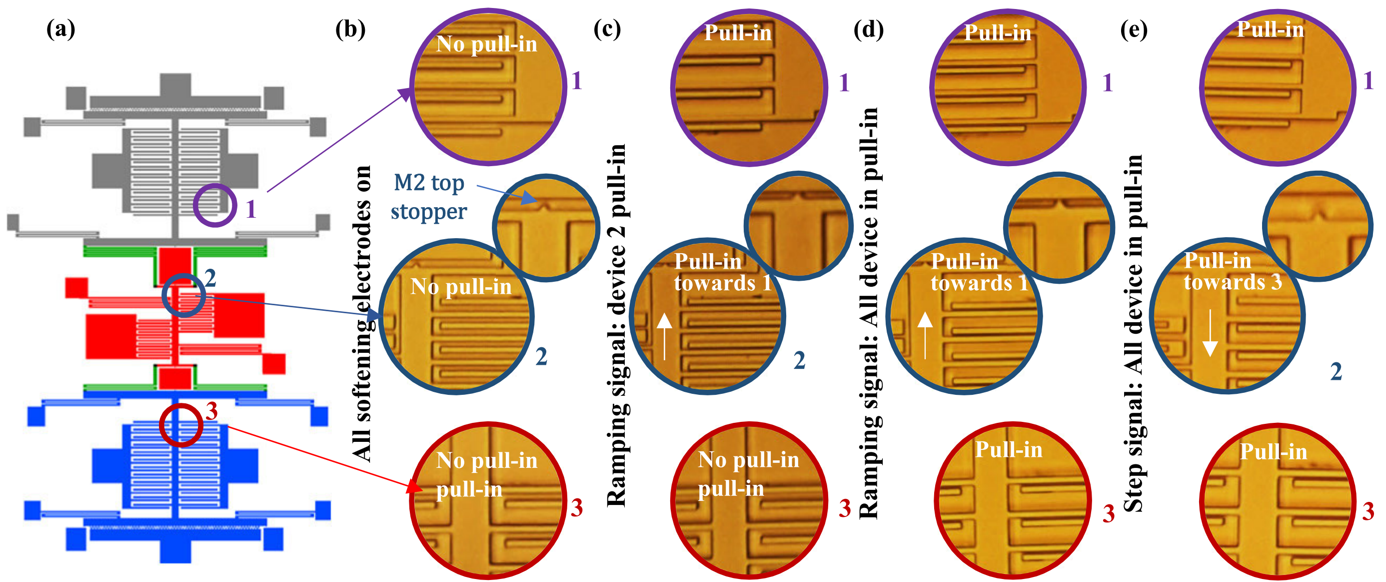

Fig. 9. Schematic views of the three coupled MEMS devices operating to perform the required signal classification task. (a) Devices are at rest. (b) Bias voltages are applied to the softening electrodes bringing the three elements close to the pull-in/instability point. (c) Gradually increasing (ramp) input voltage applied to comb drives; M2 pulled toward M1 upon M1 pull-in. (d) Ramp signal continued: eventually, M3 will pull in, but due to strong hysteresis in the parallel-plate electrostatic force (memory), M2 will not release. (e) Abruptly increasing the input voltage applied to the comb drives: both M1 and M2 are pulled-in simultaneously and M3 is pulled toward the element with which it has a stiffer coupling (down toward M1).

TABLE I
MATHEMATICAL MODEL'S PARAMETERS

Index	Unit	Description	Value
			Mathematical Model
i	non	The MEMS index	*1 – Upper mass* *2 – Middle mass* *3 – Lower mass*
x_i	$[m]$	MEMS i displacement	
m_i	$[\mu g]$	MEMS i mass	$m_1 = m_3 = 2.8892,$ $m_2 = 1.864$
c_i	$[\mu N.s/m]$	MEMS i damping constant	$c_1 = c_2 = c_3 = 13.753$
k_i	$[N/m]$	MEMS i linear stiffness coupling MEMS i with ground	$k_1 = 17, k_2 = 5.44,$ $k_3 = 20.4$
k_{ij}	$[N/m]$	MEMS i linear stiffness coupling MEMS i with MEMS j	$k_{12} = 6.12, k_{32} = 10.88$
N_{CDi}	non	Number of Comb-Drive fingers coupled with MEMS i	$N_{CD1} = N_{CD3} = 60$
g_{CDi}	$[\mu m]$	The horizontal gap between Comb-Drive finger and the MEMS i fingers	$g_{CD1} = g_{CD3} = 5$
d_{CDi}	$[\mu m]$	The vertical gap between Comb-Drive finger and the MEMS i mass	$d_{CD1} = d_{CD3} = 5$
w_{CDi}	$[\mu m]$	Width of Comb-drive finger of MEMS i	$w_{CD1} = w_{CD3} = 2$
N_{PPi}	non	Number of Parallel-plates electrodes coupled with MEMS i	$N_{PP1} = N_{PP3} =$ $24, N_{PP2} = 14$
L_{PPi}	$[\mu m]$	Length of Parallel-Plates electrodes of MEMS i	$L_{PP1} = L_{PP3} =$ $215, L_{PP2} = 191$
d_{PPUi}	$[\mu m]$	Upper gap of the Parallel-Plates electrodes of MEMS i	$d_{PPU1} = 8, d_{PPU2} = 7.03,$ $d_{PPU3} = 15$
d_{PPLi}	$[\mu m]$	Lower gap of the Parallel-Plates electrodes of MEMS i	$d_{PPL1} = 15, d_{PPL2} =$ $6.97, d_{PPL3} = 8$
V_{CDi}	$[V]$	The input voltage applied between the Comb-Drive and mass i	
V_{PPi}	$[V]$	The bias voltage applied between the Parallel-Plates and mass i	
V_r	non	$R_{CD} = V_{CD3}/V_{CD1}$	

the input ratio R_{CD} to 0.9, the network output is the same for the two different signals.

It is worth mentioning that while the bias voltages for operation are relatively high, the MEMS parameter design can

Authorized licensed use limited to: University of Nebraska Omaha Campus. Downloaded on November 06,2023 at 19:05:53 UTC from IEEE Xplore. Restrictions apply.

TABLE II
POWER CALCULATION ESTIMATION

	L	Area (L*DL)	Gap size 1	Gap size 2	Number of gaps	C1	C2	Vbias	Energy
softening 1	2.15E-04	1.08E-08	3.50E-06	1.95E-05	24	2.72E-14	4.88E-15	38	5.56E-10
softening 3	2.15E-04	1.08E-08	3.50E-06	1.95E-05	24	2.72E-14	4.88E-15	34	4.45E-10
Comb-drives 1	7.50E-06	3.75E-10	4.50E-06	3.25E-06	118	7.38E-16	1.02E-15	72	5.38E-10
Comb-drive 3	7.50E-06	3.75E-10	4.50E-06	3.25E-06	118	7.38E-16	1.02E-15	72	5.38E-10
Softening 2	1.91E-04	9.55E-09	3.00E-06	1.00E-05	14	2.82E-14	8.46E-15	33	2.79E-10
Sum									2.36E-09
									J

be optimized to reduce them. An intricate system governs the voltages needed for each element to operate in the desired fashion. As seen in (4)–(6), many factors could alter V_{PP} and V_{CD}. For the comb-drive actuators, for example, if the number of fingers increased or the gaps between the fingers decreased, the actuator would exert more force by applying the same voltage or it can run at lower voltages and still provide the desired force necessary for the device operation. The same is true for the parallel-plate electrodes. For instance, the length and the number of electrodes could be increased, so the device could operate at lower voltages. Lowering the mechanical stiffness of the structure is another avenue toward reaching lower operating voltage. For example, according to (4), if the number of fingers on the comb-drive actuator were to double, the actuator could exert the same force by applying the same voltage divided by a square root of 2 ($\sim$0.7 of the initial voltage applied). More importantly, due to the capacitive electrostatic actuation, the total energy consumed in each classification cycle is insignificant. The only energy needed to operate the described devices is the energy needed to charge the capacitances associated with the electrostatic actuators. When elements are in a pull-in stance, all the electrodes and actuators store energy based on their capacitance and the applied voltage. As an example, Table II (Appendix) shows the energy consumption of each element and the total energy consumed when all elements are in pull-in. The capacitance was calculated based on the geometry of the design, and the applied voltage is the actual operating voltage used in Fig. 9.

V. CONCLUSION AND FUTURE WORK

A three-neuron mechanically coupled MEMS network was designed to perform a classification task to distinguish between step and ramp input signals. A mathematical model to simulate the system's behavior was implemented. Following the simulation results, mechanically coupled MEMS hardware was fabricated and experimentally tested for some of the operation conditions reported in the simulation. The hardware successfully performed the classification task without needing any digital computing unit. The fact that only dc bias voltages are needed to operate this electrostatically driven device performing neural computing opens the door wide for more sophisticated ultralow-power computing units.

Future work includes adding more neurons to the micromechanical network to increase its complexity and applying machine learning training algorithms, such as the gradient-based method, to train larger MEMS hardware to solve more complex classification problems. Finally, direct sensing capabilities can be integrated within such computing units as acceleration measurements.

APPENDIX

See Tables I and II.

REFERENCES

[1] M. P. Frank, "Approaching the physical limits of computing," in *Proc. 35th Int. Symp. Multiple-Valued Log. (ISMVL)*, 2005, pp. 168–185.
[2] V. Intaraprasonk and S. Fan, "Nonvolatile bistable all-optical switch from mechanical buckling," *Appl. Phys. Lett.*, vol. 98, no. 24, Jun. 2011, Art. no. 241104.
[3] B. Ilic, Y. Yang, K. Aubin, R. Reichenbach, S. Krylov, and H. Craighead, "Enumeration of DNA molecules bound to a nanomechanical oscillator," *Nano Lett.*, vol. 5, no. 5, pp. 925–929, 2005.
[4] G. Rebeiz, *RF MEMS: Theory Design and Technology*. Hoboken, NJ, USA: Wiley, 2003.
[5] S. Ilyas, A. Ramini, A. Arevalo, and M. I. Younis, "An experimental and theoretical investigation of a micromirror under mixed-frequency excitation," *J. Microelectromech. Syst.*, vol. 24, no. 4, pp. 1124–1131, Aug. 2015.
[6] D. Antonio, D. H. Zanette, and D. López, "Frequency stabilization in nonlinear micromechanical oscillators," *Nature Commun.*, vol. 3, no. 1, p. 806, May 2012.
[7] B. Halg, "On a micro-electro-mechanical nonvolatile memory cell," *IEEE Trans. Electron Devices*, vol. 37, no. 10, pp. 2230–2236, Oct. 1990.
[8] M. A. A. Hafiz, L. Kosuru, and M. I. Younis, "Microelectromechanical reprogrammable logic device," *Nature Commun.*, vol. 7, no. 1, p. 11137, Mar. 2016.
[9] G. M. Rebeiz and J. B. Muldavin, "RF MEMS switches and switch circuits," *IEEE Microw. Mag.*, vol. 2, no. 4, pp. 59–71, Dec. 2001.
[10] E. E. Flater, A. D. Corwin, M. P. de Boer, and R. W. Carpick, "In situ wear studies of surface micromachined interfaces subject to controlled loading," *Wear*, vol. 260, no. 6, pp. 580–593, Mar. 2006.
[11] Z. Yapu, "Stiction and anti-stiction in MEMS and NEMS," *Acta Mechanica Sinica*, vol. 19, no. 1, pp. 1–10, Feb. 2003.
[12] W. M. V. Spengen, R. Puers, and I. D. Wolf, "A physical model to predict stiction in MEMS," *J. Micromech. Microeng.*, vol. 12, no. 5, pp. 702–713, Sep. 2002.
[13] I. M. M. Mahboob, K. Nishiguchi, A. Fujiwara, and H. Yamaguchi, "A multimode electromechanical parametric resonator array," *Sci. Rep.*, vol. 4, no. 1, p. 4448, 2014.
[14] F. Alsaleem, M. Younis, and R. Laura, "An experimental and theoretical investigation of dynamic pull-in in MEMS resonators actuated electrostatically," *J. Microelectromech. Syst.*, vol. 19, no. 4, pp. 794–806, 2010.
[15] M. Emad-Ud-Din, M. H. Hasan, R. Jafari, S. Pourkamali, and F. Alsaleem, "Simulation for a mems-based CTRNN ultra-low power implementation of human activity recognition," *Frontiers Digit. Health*, vol. 3, Sep. 2021, Art. no. 731076.
[16] C. Mead, "Neuromorphic electronic systems," *Proc. IEEE*, vol. 78, no. 10, pp. 1629–1636, Oct. 1990.
[17] F. C. Hoppensteadt and E. M. Izhikevich, "Synchronization of MEMS resonators and mechanical neurocomputing," *IEEE Trans. Circuits Syst. I, Fundam. Theory Appl.*, vol. 48, no. 2, pp. 133–138, Feb. 2001.
[18] A. Kumar and P. Mohanty, "Autoassociative memory and pattern recognition in micromechanical oscillator network," *Sci. Rep.*, vol. 7, no. 1, pp. 1–9, Mar. 2017.

Authorized licensed use limited to: University of Nebraska Omaha Campus. Downloaded on November 06,2023 at 19:05:53 UTC from IEEE Xplore. Restrictions apply.

[19] F. M. Alsaleem, M. H. H. Hasan, and M. K. Tesfay, "A MEMS nonlinear dynamic approach for neural computing," *J. Microelectromech. Syst.*, vol. 27, no. 5, pp. 780–789, Oct. 2018, doi: 10.1109/JMEMS.2018.2864175.

[20] M. H. Hasan et al., "Exploiting pull-in/pull-out hysteresis in electrostatic MEMS sensor networks to realize a novel sensing continuous-time recurrent neural network," *Micromachines*, vol. 12, no. 3, p. 268, Mar. 2021.

[21] M. Rafaie, M. H. Hasan, and F. M. Alsaleem, "Neuromorphic MEMS sensor network," *Appl. Phys. Lett.*, vol. 114, no. 16, Apr. 2019, Art. no. 163501.

[22] M. H. Hasan, A. Al-Ramini, E. Abdel-Rahman, R. Jafari, and F. Alsaleem, "Colocalized sensing and intelligent computing in micro-sensors," *Sensors*, vol. 20, no. 21, p. 6346, Nov. 2020, doi: 10.3390/s20216346.

[23] B. Barazani, G. Dion, J.-F. Morissette, L. Beaudoin, and J. Sylvestre, "Microfabricated neuroaccelerometer: Integrating sensing and reservoir computing in MEMS," *J. Microelectromech. Syst.*, vol. 29, no. 3, pp. 338–347, Jun. 2020, doi: 10.1109/JMEMS.2020.2978467.

[24] K. Nakada, S. Suzuki, E. Suzuki, Y. Terasaki, T. Asai, and T. Sasaki, "An information theoretic parameter tuning for MEMS-based reservoir computing," *Nonlinear Theory Appl., IEICE*, vol. 13, no. 2, pp. 459–464, 2022.

[25] C. Borra, C. S. Pyles, B. A. Wetherton, D. D. Quinn, and J. F. Rhoads, "The dynamics of large-scale arrays of coupled resonators," *J. Sound Vibrat.*, vol. 392, pp. 232–239, Mar. 2017.

[26] S. T. Habermehl, N. Bajaj, S. Y. Shah, D. D. Quinn, D. Weinstein, and J. F. Rhoads, "Synchronization in a network of coupled MEMS-Colpitts oscillators," *Nonlinear Dyn.*, vol. 98, no. 4, pp. 3037–3050, Dec. 2019.

[27] B. Peng, K.-M. Hu, X.-Y. Fang, X.-Y. Li, and W.-M. Zhang, "Modal characteristics of coupled MEMS resonator array under the effect of residual stress," *Sens. Actuators A, Phys.*, vol. 333, Jan. 2022, Art. no. 113236.

[28] F. Xue et al., "Piezoelectric-piezoresistive coupling MEMS sensors for measurement of electric fields of broad bandwidth and large dynamic range," *IEEE Trans. Ind. Electron.*, vol. 67, no. 1, pp. 551–559, Jan. 2020.

[29] M. Ghommem, V. Puzyrev, R. Sabouni, and F. Najar, "Deep learning for gas sensing using MOFs coated weakly-coupled microbeams," *Appl. Math. Model.*, vol. 105, pp. 711–728, May 2022.

[30] M. Lyu et al., "Exploiting nonlinearity to enhance the sensitivity of mode-localized mass sensor based on electrostatically coupled MEMS resonators," *Int. J. Non-Linear Mech.*, vol. 121, May 2020, Art. no. 103455.

[31] F. C. Hoppensteadt and E. M. Izhikevich, *Weakly Connected Neural Networks*, vol. 126. Berlin, Germany: Springer, 1997.

[32] K. Vandoorne et al., "Toward optical signal processing using photonic reservoir computing," *Opt. Exp.*, vol. 16, pp. 11182–11192, Jul. 2008.

[33] H. Nikfarjam et al., "Signal classification using a mechanically coupled MEMS neural network," in *Proc. IEEE Sensors*, Oct. 2021, pp. 1–4, doi: 10.1109/SENSORS47087.2021.9639616.

[34] H. Nikfarjam, S. Sheikhlari, and S. Pourkamali, "Stiction reduction in MEMS fabrication via naphthalene sublimation," in *Proc. IEEE Sensors*, Dallas, TX, USA, Oct. 2022, pp. 1–4, doi: 10.1109/SENSORS52175.2022.9967274.

[35] M. Younis, *MEMS Linear and Nonlinear Statics and Dynamics*, vol. 20. Springer, 2011.

Hamed Nikfarjam (Member, IEEE) received the B.S. degree in mechanical engineering from the University of Tehran, Tehran, Iran, in 2014. He is pursuing the Ph.D. degree with the Department of Electrical Engineering, The University of Texas at Dallas, Richardson, TX, USA.

He is also a Researcher with the MicroneX Laboratory, The University of Texas at Dallas. His research interests include integrated silicon-based micro-electromechanical systems (MEMS) and microsystems, micro/nano fabrication technologies, accelerometers, and machine learning using MEMS.

Mr. Nikfarjam was recognized for his outstanding research contributions and was awarded the prestigious Jan Van der Ziel Fellowship for the 2023–2024 academic year at The University of Texas at Dallas.

Mohammad Megdadi received the bachelor's degree in mechanical engineering from the Jordan University of Science and Technology (JUST), Ar-Ramtha, Jordan, in 2020. He is pursuing the Ph.D. degree in mechanical engineering with the University of Nebraska–Lincoln (UNL), Lincoln, NE, USA.

His main research fields are micro-electromechanical systems (MEMS), neuromorphic computing, machine learning, modeling, and 3-D design.

Mohammad Okour received the B.Sc. and master's degrees in mechanical engineering from the Jordan University of Science and Technology, Ar-Ramtha, Jordan, in 2018 and 2021, respectively. He is pursuing the Ph.D. degree with the University of Nebraska–Lincoln, Lincoln, NE, USA.

His areas of interest include control systems applications, artificial intelligence, machine learning, system dynamics, vibration analysis, and micro-electromechanical systems (MEMS).

Siavash Pourkamali (Senior Member, IEEE) received the B.S. degree in electrical engineering from the Sharif University of Technology, Tehran, Iran, in 2001, and the M.S. and Ph.D. degrees in electrical engineering from the Georgia Institute of Technology, Atlanta, GA, USA, in 2004 and 2006, respectively.

He is a Professor with the Department of Electrical Engineering and Computer Sciences, The University of Texas at Dallas (UT-Dallas), Richardson, TX, USA. Prior to joining UT-Dallas in 2012, he was an Assistant Professor with the University of Denver, Denver, CO, USA. Prof. Pourkamali's current research interests are in the area of integrated silicon-based micromachined transducers and microsystems.

Prof. Pourkamali was a recipient of the 2011 National Science Foundation CAREER Award, the 2008 University of Denver Best Junior Scholar Award, and the 2006 Georgia Tech Electrical and Computer Engineering Research Excellence Award.

Fadi Alsaleem received the M.S. and Ph.D. degrees from the Department of Mechanical Engineering, State University of New York at Binghamton, Binghamton, NY, USA, in 2007 and 2009, respectively.

He is an Associate Professor with the Department of Architectural Engineering at the University of Nebraska-Lincoln, Lincoln, NE. Previously, he worked as an Assistant Professor at the Wichita State University, Wichita, KS, from 2015 to 2016. Before these assignments, Dr. Alsaleem worked for four years as a Senior Lead Algorithm Engineer with Emerson Climate Technology, Sidney, OH, a business of Emerson, the world's leading provider of heating, air conditioning, and refrigeration solutions for residential, industrial, and commercial applications. He joined MicrostaQ Inc., Austin, TX, USA, for two years as a Micro-Electro-Mechanical Systems (MEMS) Control Engineer. He has been an Active Researcher in the area of nonlinear dynamics of MEMS, smart MEMS, the Internet of Things (IoT), smart building, online monitoring and diagnostics, and big data analysis.

Dr. Alsaleem has received more multimillion in research grants from many diverse sources of funding, including the National Science Foundation (NSF) collaborative grant (Lead P.I.), the Department of Energy (DOE), the Intelligence Advanced Research Projects Activity (IARPA) Grant, and industry grants. He also received the UNL College of Engineering Faculty Research and Creative Activity Award in 2022.

Authorized licensed use limited to: University of Nebraska Omaha Campus. Downloaded on November 06,2023 at 19:05:53 UTC from IEEE Xplore. Restrictions apply.